Supplemental Document

Biomedical Optics EXPRESS

Axial motion estimation and correction for simultaneous multi-plane two-photon calcium imaging: supplement

ANDRES FLORES-VALLE[1,2,3] AND JOHANNES D. SEELIG[1,4]

[1] *Max Planck Institute for Neurobiology of Behavior – caesar (MPINB), Bonn, Germany*
[2] *International Max Planck Research School for Brain and Behavior, Bonn, Germany*
[3] *andres.flores@mpinb.mpg.de*
[4] *johannes.seelig@mpinb.mpg.de*

Supplement DOI: https://doi.org/10.6084/m9.figshare.19137050

Parent Article DOI: https://doi.org/10.1364/BOE.445775

Supplement 1: Methods

Microscope setup

The setup was described in [23]. Briefly, two axially offset Gaussian beams were used to record in two different focal planes using temporal multiplexing [18]. Temporal multiplexing was performed using Scanimage in photon counting mode [14]. The diameter and collimation of each beam was adjusted with two lenses (Thorlabs achromatic doublets), while the two beams were linearly and orthogonality polarized and delayed by $2m$, as shown in Fig. 1B. The beams were focused at the samples with a power of $6mW$ for each beam by underfilling the objective of the microscope (16X Nikon CFI LWD Plan Fluorite Objective, 0.80 NA, 3.0 mm WD). This created elongated beam profiles along the axial direction (Fig. 1). The full width at half maximum was adjusted to $9\mu m$ and $16\mu m$ (computed from the standard deviations: FWHM = 2.4σ), respectively, and the peaks of the two beams were separated by $7\mu m$.

Drosophila preparation

Imaging in behaving flies we performed as described in [23]. Briefly, We used 7-10 days old female flies, either expressing GFP or GCaMP8f in wedge neurons (R60D05-GAL4). We performed laser surgery to remove the cuticle over the brain. The cuticle and underlying tissue were then removed either with a microrobotic arm or manually under a dissection scope [23]. Finally, a drop of glue was placed on the opening (DETAX, Freeform, 02204). The flies expressing GCaMP8f were left to recover over night [23], while flies expressing GFP were imaged directly after surgery.

For the fly expressing GFP, as well as for the fly in Fig. 6 the proboscis was fixed with wax to prevent brain motion [7]. For imaging, flies were glued to a cover slide ((22 mm × 22 mm, thickness No. 1, Cat. No. 631-0124, see [23] for details of the preparation).

Extracting head direction from calcium signals

We computed the trajectory of the bump of activity along the ROIs, $b(t)$, based on the ROI position with maximum fluorescence value of the corrected $\Delta F/F$:

$$b(t) = argmax_i \Big[\quad \text{corrected} \quad \Delta F/F_i(t) \quad \Big] \tag{6}$$

We then used this trajectory to compute the bump amplitude in both, measured and corrected $\Delta F/F$, in the ROIs along the bump trajectory:

$$\begin{cases} \text{corrected bump amplitude}(t) = \text{corrected} \quad \Delta F/F_{b(t)}(t) \\ \text{measured bump amplitude}(t) = \text{measured} \quad \Delta F/F_{b(t)}(t) \end{cases} \tag{7}$$

Analytical approximation of motion correction algorithm for a single ROI

While motion correction was performed numerically as described in Algorithm 1, we here first explain the operation of the algorithm using an analytical approximation, assuming continuous time and z-axis, first for a single ROI defined on a 3D sample in the absence of noise.

A single ROI is a voxel extended along the z-axis, which is described as a function $e(A, z)$ representing the number of fluorescent proteins, for example GFP or GCaMP, inside the ROI at a given z position. The function $e(A, z)$ changes over time depending on a variable A, $A = A(t)$, representing neural activity in each ROI. Generally, the ROI function, $e(A, z)$, could have any form. As an example, Fig. S1A shows a ROI function defined by the following Eq.:

$$e(A, t) = A \exp\left[\frac{(z + p_1)^2}{2\sigma^2}\right] + A^2 \exp\left[\frac{(z + p_2)^2}{2\sigma^2}\right], \tag{8}$$

where $p_1 = -5\mu m$ and $p_2 = 5\mu m$ represent the center of two Gaussians with standard deviation $\sigma = 2.5\mu m$. In this case the activity A changes the Gaussian peaks by different amplitudes (Fig. S1A), meaning that fluorescence changes heterogeneously at different z positions. This could for example be the case if two different dendrites of a neuron receive inputs with different strengths.

To simplify the problem of motion estimation and correction, we can approximate the ROI function to first order with a Taylor series around $A = 0$:

$$e(A, z) \approx e(0, z) + \frac{\partial e(A, z)}{\partial A}\Big|_{A=0} A. \tag{9}$$

The derivative of $e(A, z)$ with respect to A and evaluated at $A = 0$ is a function that only depends on z, which we call $\rho(z)$. On the other hand, $e(0, z)$ is the baseline fluorescence indicator distribution along the z-axis which is not modulated by the activity A of the ROI. We assume for simplicity that $e(0, z)$ is negligible, assuming that there is an activity baseline, A^0, much larger than $e(0, z)$:

$$A^0\rho(z) \quad >> \quad e(0, z) \tag{10}$$

With this approximation, we can write the ROI function as:

$$e(A, z) = A\rho(z) \tag{11}$$

The function $\rho(z)$ describes a density of fluorescence proteins along the z-axis, while A increases activity inside the ROI homogeneously. In the following we refer to $\rho(z)$ as the ROI density while A is called the ROI activity. An example of Eq. (11) is given in Fig. S1B, where $\rho(z)$ is defined by the following expression:

$$\rho(z) = \exp\left[\frac{(z + p_1)^2}{2\sigma^2}\right] + \exp\left[\frac{(z + p_2)^2}{2\sigma^2}\right] \tag{12}$$

In addition, we assume that the ROI undergoes axial (along the z-axis) motion, described with a time-dependent variable, $\Delta z(t)$, which changes the offset of the ROI density along the z-axis. Assuming no distortion in the sample during axial motion, the ROI density remains constant but moves along the z-axis. Therefore, the ROI function is finally approximated as:

$$e(t, z) = A(t)\rho(z - \Delta z(t)) \tag{13}$$

Eq. (13) allows us to separate the ROI function, $e(t, z)$, into two parts, one which depends on the activity of the ROI, $A(t)$, which is independent of the z-axis, and another one that depends on the motion of the sample, $\rho(z - \Delta z(t))$.

This first order approximation, which was valid in the biological samples used for the experiments, allows us to develop an algorithm to estimate and correct the axial motion of the sample. The goal of the algorithm is to estimate axial motion, $\Delta z(t)$, as well as to extract the activity, $A(t)$.

The ROI activity is measured using two beams described by two functions, $g_1(z)$ and $g_2(z)$, which represent the shape of the beams along the z-axis. For the algorithm to work, these two beams must have different profiles along the z-axis (to provide unique information about the sample) and must be integrable, meaning that their integral must be finite. In practice, we assume that these are Gaussian beams centered at different positions along the z-axis, while their width along the z-axis and power can be different. At each time, t, both beams excite the sample with a time delay (on the order of the fluorescence lifetime), and produce two independently measured fluorescence signals.

The intensity of each fluorescence signal associated with each beam, $I_1(t)$ and $I_2(t)$, is the integral of the excitation of each beam within the ROI along the z-axis:

$$\begin{cases} I_1(t) = \int_{-\infty}^{\infty} e(t,z) g_1(z) dz \\ \\ I_2(t) = \int_{-\infty}^{\infty} e(t,z) g_2(z) dz. \end{cases} \tag{14}$$

Since the ROI activity, $A(t)$, is independent of z (Eq. (13)), we can write the measured intensities as:

$$\begin{cases} I_1(t) = A(t) G_1(\Delta z(t)) \\ I_2(t) = A(t) G_2(\Delta z(t)), \end{cases} \tag{15}$$

where G_1 and G_2 are two functions defined by the integral over the excitation of each beam at the ROI density, $\rho(z - \Delta z(t))$, and only depend on the axial motion of the sample, $\Delta z(t)$. Eq. (15) describes how changes in the measured intensities, $I_1(t)$ and $I_2(t)$, can have two different contributions: the activity of the ROI and the axial motion of the sample.

For estimating axial motion of the sample, $\Delta z(t)$, a calibration step is first performed. At the beginning of the experiment ($t = 0$), a z-stack is recorded with each beam by moving the two beams simultaneously and continuously along the z-axis. We assume that the ROI activity and axial motion of the sample, $A(0)$ and $\Delta z(0)$, do not change when recroding the stack. Moreover, and without loss of generality, we define the origin of the axial motion while recording the stacks so that $\Delta z(0) = 0$. In practice, the assumption that $A(0)$ and $\Delta z(0)$ do not change is achieved by averaging over several stacks (see Results with biological samples expressing GFP or GCaAMP8f). The algorithm however works with arbitrary activity $A(0)$ during z-stack acquisition. Since moving the beams is equivalent to moving the sample in the opposite direction while leaving the beams fixed, the stacks are defined as follows:

$$\begin{cases} I_1^{(stack)}(z) = A(0) \int_{-\infty}^{\infty} \rho(z' - z) g_1(z') dz' \\ \\ I_2^{(stack)}(z) = A(0) \int_{-\infty}^{\infty} \rho(z' - z) g_2(z') dz' \end{cases} \tag{16}$$

This equation can be expressed as

$$\begin{cases} I_1^{(stack)}(z) = A(0) G_1(z) \\ I_2^{(stack)}(z) = A(0) G_2(z) \end{cases} \tag{17}$$

The ratios $I_1(t)/I_2(t)$ and $I_1^{stack}(z)/I_2^{stack}(z)$ do not depend on the activity and we use this to define the following cost function,

$$J_{L_2}(z,t) = \left(\frac{I_1(t)}{I_2(t)} - \frac{I_1^{stack}(z)}{I_2^{stack}(z)} \right)^2 = \left(\frac{G_1(\Delta z(t))}{G_2(\Delta z(t))} - \frac{G_1(z)}{G_2(z))} \right)^2 \tag{18}$$

The cost function $J_{L_2}(z)$ is minimized at time t when $z = \Delta z(t)$. This optimization is used to find the axial motion of the sample, $\Delta z(t)$, using the stacks. We will show in the following sections (Eq. (1)) that the shape of this cost function arises from a expectation–maximization approach. To take into account that the axial motion of the sample is correlated in time, we modified Eq. (18), with a Gaussian filter over time:

$$J_{L_2}(z,t) = \int_{-\infty}^{\infty} f(t' - t, \sigma_t) \left(\frac{I_1(t)}{I_2(t)} - \frac{I_1^{stack}(z)}{I_2^{stack}(z)} \right)^2 dt' \tag{19}$$

where $f(t-t',\sigma)$ is a Gaussian kernel centered at time t with standard deviation σ_t, defined as:

$$f(t'-t,\sigma) = \exp\Big[-\frac{(t'-t)^2}{2\sigma_t^2}\Big] \tag{20}$$

Eq. (19) provides a filtered estimate of the axial motion of the sample by weighting contributions from several intensity measurements. This cost function assumes that changes in axial motion within the Gaussian kernel are small. The standard deviation, σ_t, is a manually-set parameter that provides the size of the time window considered for the axial motion estimation.

To find the axial motion of the sample at any time t, we find the z-position in the stack, $\hat{z}(t)$, that minimizes the cost function.

$$\hat{z}(t) = \text{argmin}_z\Big[\quad J(z,t)\quad\Big] \tag{21}$$

The value of the cost function evaluated at the estimated displacement, $\hat{z}(t)$, provides a measure for the quality of the optimisation result at time t.

$$\text{cost function error}(t) = J(\hat{z}(t),t) \tag{22}$$

Once the the motion of the sample is estimated, we correct the measured intensities by dividing the intensity recorded by each beam by its corresponding stack, evaluated at the estimated slice $\hat{z}(t)$ at any time t:

$$\begin{cases} I_1^{cor}(t) = \frac{I_1(t)}{I_1^{stack}(\hat{z}(t))} = \frac{A(t)}{A(0)}\frac{G_1(\Delta z(t))}{G_1(\hat{z}(t))} \\ \\ I_2^{cor}(t) = \frac{I_2(t)}{I_2^{stack}(\hat{z}(t))} = \frac{A(t)}{A(0)}\frac{G_2(\Delta z(t))}{G_2(\hat{z}(t))} \end{cases} \tag{23}$$

This correction eliminates the contribution of the axial motion of the sample from the measured intensities if the axial motion estimation is correct, i.e. $\hat{z}(t) = \Delta z$, leaving only the contributions made by changes in the activity $A(t)$. Finally we can compute the relative change in fluorescence, $\Delta F/F$, using the corrected intensities:

$$\Delta F/F(t) = \frac{1}{2}\Big(\frac{I_1^{cor}(t)-F_1^0}{F_1^0} + \frac{I_2^{cor}(t)-F_2^0}{F_2^0}\Big) = \frac{A(t)-A^0}{A^0} \tag{24}$$

where F_1^0 and F_2^0 are the baselines of the intensities $I_1^{cor}(t)$ and $I_2^{cor}(t)$ respectively, corresponding to the ROI activity baseline, A^0. The baselines F_1^0 and F_2^0 are obtained by computing the mean value of the lowest 10% values of the corrected intensities, I_1^{cor} and I_2^{cor}, respectively.

Simulation of a moving single ROI

To demonstrate how this algorithm works for a single ROI, we simulated a single ROI along the z-axis described by Eq. (11) with an activity density defined as

$$\rho(z) = \begin{cases} \frac{2}{3} + \frac{1}{3}\sin\Big[(z-z_0)\frac{\pi}{L}\Big] & \text{if} \quad z_0 > z > z_0 + L \\ 0 & \text{otherwise,} \end{cases} \tag{25}$$

where $z_0 = -5\mu m$ and $L = 10\mu m$. The ROI undergoes axial motion over time, as defined by Eq. (13) and shown in Fig. 2B, described by the following Eq.:

$$\Delta z(t) = z_{amp}\sin(2\pi f_z t) \tag{26}$$

where $z_{amp} = 5\mu m$ and $f_z = 5Hz$ are the amplitude and frequency of a simulated sinusoidal axial motion. The activity of the sample, $A(t)$, is modeled by a differential Eq.:

$$\tau_A \dot{A}(t) = -A(t) + 1 + \epsilon_A, \tag{27}$$

where $\tau_A = 10ms$ is a time constant, and ϵ_e is a stochastic input to the sample that produces spikes along the simulation with 0.5% probability and positive amplitude.

To record the activity of the sample, we defined two beams with Gaussians axial profiles, according to the following equation:

$$g_i(z) = C_i e^{-(z-d_i)^2/(2\sigma_i^2)} \qquad \text{for } i = 1, 2, \tag{28}$$

where $C_1 = 1.25a.u.$ and $C_2 = 1.5a.u.$ define the maximum beam power and $\sigma_1 = 2\mu m$ and $\sigma_2 = 3\mu m$ are the widths (standard deviations) along the z-axis. The two beams are offset in axial direction, $d_1 = -2.5\mu m$ and $d_2 = 2.5\mu m$. The shape of the beams is shown at the top of Fig. 2A, together with the ROI function at time $t = 0$, $e(0, z)$.

A z-stack of the sample at time $t = 0$ is defined in the absence of axial motion, $\Delta z(0) = 0$, and activity is defined as $A(0) = 1$. The stack is simulated by recording the activity of the sample while moving the beams along the the z-axis from $-25\mu m$ to $25\mu m$ in steps of $0.05\mu m$, resulting in a convolution between the beams and the sample according to Eq. (16) (Fig. 2A). Only a single stack without averaging is used for simulations.

Next, combined sample motion and activity are simulated for 1000 milliseconds. The equation for the activity, $A(t)$, is solved using forward Euler with a time step of $dt = 0.001$ milliseconds. The intensity of each beam is given by Eq. (14). The result of the simulation is shown in Fig. 2C, where the first row shows the moving sample and its activity, and the second row shows the intensities recorded in each beam.

To estimate sample motion, $\hat{z}(t)$, at each instant t, we computed the value of the cost function (Eq. (19)) at all z positions of the stacks (from $-25\mu m$ to $25\mu m$ in steps of $0.05\mu m$). Finally, motion at time t, $\Delta z(t)$, is estimated according to Eq. (21), by finding the position $\hat{z}$ that minimizes the cost function across all z values. The third row in Fig. 2B shows the real versus the estimated motion of the sample. The error of the optimisation process is calculated using Eq. (22) and shown in the fourth row of Fig. 2.

Finally, the recorded intensities are corrected using the estimated axial motion and Eq. (23), and changes in fluorescence intensity, $\Delta F/F$, are computed from the corrected intensities, according to Eq. (24). The last row in Fig. 2 shows the actual and the corrected changes in fluorescence, respectively. The actual $\Delta F/F$ is calculated according to the following Eq.:

$$\text{actual} \quad \Delta F/F = \frac{A(t) - A^0}{A^0} \tag{29}$$

where A^0 is an activity baseline calculated as the average of the lowest 10% values of $A(t)$.

Algorithm for motion estimation and correction for several ROIs with noise

We now extend the approach developed above to a sample with multiple ROIs. In addition we now consider that the measurements are noisy. We assume rigid three-dimensional sample motion, with negligible elastic deformations or changes in orientation.

We record a total of T pair of images, $M_1(t)$ and $M_2(t)$, one for each beam, for $t = 1, ..., T$ and assume that all images are aligned, that is, corrected for lateral motion. We define N ROIs on the images and each ROI i describes an area on the images containing n_i pixels. The sum of the values of all the pixels of each image inside this area, $M_1^{(w,h)}(t)$ and $M_1^{(w,h)}(t)$, where $(w, h) \in$ ROI i, provides a pair of intensity measurements of the ROI i in each pair of images at time t:

$$\begin{cases} I_{1,i}(t) = \sum_{(w,h)\in ROI_i} M_1^{(w,h)}(t) \\ I_{2,i}(t) = \sum_{(w,h)\in ROI_i} M_2^{(w,h)}(t). \end{cases} \tag{30}$$

The fluorescence signals detected by the PMT are subjected to shot noise and the intensities in each pixel follow independent Poisson distributions. If the number n_i of pixels in each ROI i is large, each pair of intensity measurements approaches the following normal distributions:

$$\begin{cases} I_{1,i}(t) \sim \mathcal{N}\Big(\mu_{1,i}(t), \mu_{1,i}^2(t)\Big) \\ I_{2,i}(t) \sim \mathcal{N}\Big(\mu_{2,i}(t), \mu_{2,i}^2(t)\Big) \end{cases} \tag{31}$$

where $\mu_{1,i}$ and $\mu_{2,i}$ are the means of the normal distribution for each beam, respectively.

Using the first-order Taylor expansion (Eq. (9)), we can approximate each ROI function i by the following expression:

$$e_i(t, z) = A_i(t)\rho_i(z - \Delta z(t)) \quad \text{for } i = 1, ..., N \tag{32}$$

where $A_i(t)$ and $\rho_i(z - \Delta z(t))$ are the activity and density of each ROI i, respectively, during the acquisition t. We again assume that the ROI moves in the axial direction, given by $\Delta z(t)$. Then, we can approximate the means of the intensity distributions, $\mu_{1,i}(t)$ and $\mu_{2,i}(t)$, as

$$\begin{cases} \mu_{1,i}(t) = A_i(t)G_{1,i}(\Delta z(t)) \\ \mu_{2,i}(t) = A_i(t)G_{2,i}(\Delta z(t)) \end{cases} \quad \text{for } i = 1, ..., N \quad , \tag{33}$$

where $G_{1,i}(\Delta z(t))$ and $G_{2,i}(\Delta z(t))$ are functions defined by the integral of the excitation of each beam at each ROI density, $\rho_i(z)_i$.

We now take the ratio of the intensities for each ROI i at each acquisition t, $I_{1,i}(t)/I_{2,i}(t)$, since the ratio of the mean values $\mu_{1,i}(t)/\mu_{2,i}(t)$ does not depend on the ROI acivity, $A_i(t)$. The ratio of these two normal variables is well approximated by a normal distribution around the mean of the ratio, $\mu_{1,i}(t)/\mu_{2,i}(t)$, if the means are positive and the coefficients of variation, $\delta_{1,i}(t) = \sqrt{\mu_{1,i}(t)}/\mu_{1,i}(t)$ and $\delta_{2,i}(t) = \sqrt{\mu_{2,i}(t)}/\mu_{2,i}(t)$ are smaller than 0.1 [34].

$$\frac{I_{1,i}(t)}{I_{2,i}(t)} \sim \mathcal{N}\left(\frac{\mu_{1,i}(t)}{\mu_{2,i}(t)}, \quad 2\delta_{2,i}^2(t)\Big(\frac{\mu_{1,i}(t)}{\mu_{2,i}(t)}\Big)^2\right) \tag{34}$$

Assuming that all ROIs undergo the same axial motion, Δz, we can compute the log-likelihood for the ROIs with respect to their axial position, Δz, at acquisition t:

$$L\Big(\Delta z \quad | \quad \frac{I_{1,1}(t)}{I_{2,1}(t)}, ... \frac{I_{1,N}(t)}{I_{2,N}(t)}\Big) =$$
$$-\frac{N}{2}\log(2\pi) - \frac{1}{2}\sum_{i=1}^{N}\log\Big(2\delta_{2,i}^2(t)\Big(\frac{\mu_{1,i}(t)}{\mu_{2,i}(t)}\Big)^2\Big) - \sum_{i=1}^{N}\frac{1}{\delta_{2,i}^2(t)}\Big(\frac{\mu_{2,i}(t)}{\mu_{1,i}(t)}\Big)^2\Big(\frac{I_{1,i}(t)}{I_{2,i}(t)} - \frac{\mu_{1,i}(t)}{\mu_{2,i}(t)}\Big)^2, \tag{35}$$

where the mean of the ratio distributions depends only on the axial motion $\Delta z(t)$, and not on the activity of the ROIs:

$$\frac{\mu_{1,i}(t)}{\mu_{2,i}(t)} = \frac{G_{1,i}(\Delta z(t))}{G_{2,i}(\Delta z(t))} \tag{36}$$

To compute the ratio of the means for each ROI i, we used z-stacks recorded at the beginning of the experiment, $t = 0$. Each slice in each stack is aligned to remove lateral motion using phase correction [27], and the intensity for each ROI i in each z-slice is computed, $I_{1,i}^{(stack)}(z)$ and $I_{2,i}^{(stack)}(z)$. During the acquisition of the stack, both axial motion and activity of each ROI are

considered constant, while the noise in the intensities of the slices in the stacks are assumed zero. Therefore, the intensity of each ROI in each slice of the stacks is given by the following equation:

$$\begin{cases} I_{1,i}^{(stack)}(z) = A_i(0)G_{1,i}(z) \\ I_{2,i}^{(stack)}(z) = A_i(0)G_{2,i}(z) \end{cases} \tag{37}$$

In practice, the previous assumptions are achieved by averaging several stacks and applying a median filter (see Results). We can now approximate the mean of the ratio distribution by the ratio of the intensities in the stacks at the slice Δz:

$$\frac{\mu_{1,i}(t)}{\mu_{2,i}(t)} = \frac{I_{1,i}^{(stack)}(\Delta z(t)))}{I_{2,i}^{(stack)}(\Delta z(t))}. \tag{38}$$

Finally, we can write the log-likelihood (Eq.) using the stacks as a function of z at each acquisition, t:

Note that $L(z,t)$ has a quadratic difference between the ratio of the stacks and the ratio of intensities (right side of Eq. (1)), similar to the cost function defined for a single ROI (Eq. (18)), which was minimized due to the change in sign. The log-likelihood function, however, weights (left factor on the third term in Eq. (1)) and offsets (second term in Eq. (1)) this quadratic difference, taking into account more strongly ROIs that are less noisy to estimate the axial motion, i.e., the intensity of those ROIs with lower values (and therefore lower standard deviation in their distributions).

Since axial motion is correlated in time, we use a Gaussian filter similar to Eq. (19)) in the log-likelihood: where the kernel $f(t'-t,\sigma_t)$ is defined in Eq. 20. Again, the variable σ_t is manually set, and defines the size of the time window considered for the sum of log-likelihoods.

Since the z-stacks have a finite number of slices, we can compute the value of $L_f(z,t)$ numerically for each slice z and then estimate the axial motion of the sample, $\hat{z}(t)$, at each time t, from the slice z that maximizes the log-likelihood function, $L_f(z,t)$:

$$\hat{z}(t) = \text{argmax}_z \Big[L_f(z,t) \Big]. \tag{39}$$

We provide an estimation error, $E(t)$, by computing the standard deviation of the difference between the ratio of recorded intensities and the ratio of the means:

$$E(t) = \frac{1}{N} \sum_{i=0}^{N} \Big(\frac{I_{1,i}(t)}{I_{2,i}(t)} - \frac{\mu_{1,i}(t)}{\mu_{2,i}(t)} \Big)^2 \tag{40}$$

and using Eq. (38), this error can be expressed as:

Next, we correct the measured intensities from each beam using the estimated axial motion and extending Eq. (23) to N ROIs:

This correction eliminates the axial motion contribution from the intensity measurements. However, note that this correction inherits the noise from the measured intensities $I_{1,i}(t)$ and $I_{2,i}(t)$. According to Eq. (31), both intensity corrections are obtained according to the following normal distribution:

$$\begin{cases} \hat{I}_{1,i}^{cor}(t) \sim \mathcal{N}\Big(1,1\Big) \\ \hat{I}_{2,i}^{cor}(t) \sim \mathcal{N}\Big(1,1\Big) \end{cases} \tag{41}$$

Finally, we compute the change in fluorescence for each ROI i as follows:

where $F_{1,i}^0$ and $F_{2,i}^0$ are the baselines of the intensities, $I_{1,i}^{cor}$ and $I_{2,i}^{cor}$ that correspond to the activity baseline of each ROI, A_i^0. As for the case of a single ROI, we compute the baselines $F_{1,i}^0$ and $F_{2,i}^0$ from the average of the 10% lowest values of $I_{1,i}^{cor}(t)$ and $I_{2,i}^{cor}(t)$ respectively, for each ROI i.

Simulation of several moving ROIs

We demonstrate how the algorithm works for a simulation of $N = 32$ moving ROIs with noise. In this simulation it is assumed that lateral motion of a 3D sample is already corrected and the ROIs are defined. The density of each ROI is defined along the z-axis according to the following equation:

$$\rho_i(z) = \begin{cases} \frac{1}{C_i}\left(a_i^0 + a_i^1 sin\left[(z - z_{0,i})\frac{\pi}{L_i}\right]\right) & \text{if} \quad z_{0,i} > z > z_{0,i} + L_i \\ 0 & \text{otherwise,} \end{cases} \tag{42}$$

where a_i^0 and a_i^1 are random coefficients for each ROI obtained from an uniform distribution in the range $[1, 2]$ and $z_{0,i}$ and L_i are a random origin and random length for each ROI, sampled from a uniform distribution in the range of $[-2, -5]$ and $[10, 15]$, respectively. The constant C_i normalizes the density of each ROI so that $\rho_i(z)$ is in the range of $[0, 1]$. Fig. 3A, top, shows the density of each ROI used in the simulation.

The motion of all ROIs is modeled as in the simulation in section using Eq. (26) with a frequency of $f_z = 8Hz$. The activity of each sample is modeled as:

$$\tau_A \dot{A}_i(t) = -A_i(t) + 1 + U(t, i), \tag{43}$$

where $\tau_A = 10ms$ is the time constant and $U(t, i)$ is an input defined as a rotating Gaussian along the ROIs:

$$U(t, i) = U_{max} \exp\left[- \frac{min\Big[\quad |i - v(t)|, \quad N - |i - v(t)|\Big]^2}{2\sigma^2} \quad \right] \tag{44}$$

where $U_{max} = 2$ is the amplitude, $\sigma = 2$ is the width of the Gaussian and $v(t)$ rotates the input with respect to the ROIs at a frequency of $f_u = 10Hz$, according to

$$v(t) = \quad \text{mod } (f_u N t, N), \tag{45}$$

where mod $(\cdot, \cdot)$ indicates the modulo operation. The activity of the ROIs is again solved using forward Euler with a time step of $dt = 0.001$ millisecond. An example of ROI 1 undergoing axial motion while receiving the rotating input is shown in Fig. 3A, bottom, while the rotating input in all the ROIs during the simulation is shown in Fig. 3C, fourth row.

Two beams, defined again by Eq. (28), were used to record the fluorescence change in all ROIs. At time $t = 0$ we recorded a z-stack using 1000 slices (from $-25\mu m$ to 25μ in steps of $0.05\mu m$), assuming no axial motion of the sample, $\Delta z(0) = 0$. The recorded z-stacks are shown in Fig. 3B. Note that the activity during the z-stack acquisition is higher around the ROI 16. The algorithm can estimate and correct the axial motion with arbitrary activity $A_i(0)$ in the z-stack.

After defining the stacks, the intensities at time t in two simultaneous planes for each ROI i are simulated, $I_{1,i}(t)$ and $I_{1,i}(t)$, with changing axial position and ROI activity. The intensities in each plane are sampled from a Gaussian distribution, given by Eq. (31), where the mean values $\mu_{1,i}(t)$ and $\mu_{2,i}(t)$ are computed using Eq. (33).

To estimate axial motion of the sample, $\Delta z(t)$, we computed the value of the log-likelihood function in Eq. (2) at all 1000 z positions of the stacks, at any time t, using a time window of size $\sigma_t = 3$. The estimated axial motion is then obtained by the slice in the $z-$stacks, $\hat{z}(t)$, that maximizes the log-likelihood function. The first row of Fig. 3C shows the estimated compared to the actual axial motion during the simulation, while the estimation error, computed by Eq. (3), is shown in the second row of Fig. 3C.

Next we corrected the measured intensities from each beam and each ROI using the estimated axial motion and Eq. (4). The change in fluorescence of the corrected intensities, corrected

$\Delta F/F_i(t)$, is computed using Eq. (5) and shown in Fig. 3C, fourth row. This is compared with the actual $\Delta F/F_i(t)$ (Fig. 3C, fifth row), which is computed as:

$$\text{actual} \quad \Delta F/F_i(t) = \frac{A_i(t) - A_i^0}{A_i^0}, \tag{46}$$

where A_i^0 is the baseline activity of each ROI i, obtained from the average of the 10% lowest values of $A(t)$. Fig. 3C, third row, shows the change in fluorescence measured without motion correction. This measured $\Delta F/F_i(t)$ is obtained by the following Eq.:

$$\text{measured} \quad \Delta F/F_i(t) = \frac{1}{2}\Big(\frac{I_{1,i}(t) - I_{1,i}^0}{I_{1,i}^0} + \frac{I_{2,i}(t) - I_{2,i}^0}{I_{2,i}^0}\Big), \tag{47}$$

where $I_{1,i}^0$ and $I_{2,i}^0$ are the baseline measured intensities for each beam, obtained by the mean value of the 10% lowest values of $I_{1,i}(t)$ and $I_{2,i}(t)$, respectively. These baseline values are affected by axial motion and therefore changes in fluorescence appear much larger (Fig. 3C, third row) when the sample is out of focus due to the resulting low intensities. Further, the corrected $\Delta F/F$ is larger than the actual $\Delta F/F$ (Fig. 3, fourth and fifth row). This is due to noise in the measurements, which produces lower baselines values, $F_{1,i}^0$ and $F_{2,i}^0$. These lower values follow from averaging over the lowest 10% values of the corrected intensities (see for example Fig. S2B) instead of taking the mean value of the distribution.

Simulation for motion estimation and correction with four simultaneously recorded focal planes

Here, we extend the motion correction algorithm to four beams using simulations. For simplicity we consider only a single ROI. The ROI density is defined again by Eq. (25). Four different Gaussian beams are defined, according to the following equation:

$$g_j(z) = C_j e^{-(z-d_j)^2/(2\sigma_j^2)} \qquad \text{for } j = 1, 2, 3, 4, \tag{48}$$

where $C_1 = 1, C_2 = 1.5, C_3 = 2$ and $C_4 = 0.5$ are the maximum beam powers, and $\sigma_1 = 3$, $\sigma_2 = 3$, $\sigma_3 = 2$ and $\sigma_4 = 3$ are the beam widths (standard deviations) along the z-axis. Each beam is offset from the previous one by $3.33\mu m$ ($d_1 = -5$, $d_2 = -1.67$, $d_3 = 1.67$ and $d_4 = 5$). The beam profiles, as well as the ROI densities, are shown in Fig. S4A, first row.

First, a stack is recorded by continuously moving each beam long the z axis, from $-25\mu m$ to 25μ in steps of 0.05μ. The stack obtained for each beam is shown in the second row of S4A. We assume that the ROI undergoes axial motion over time, defined by Eq. (26), while its activity changes according to (27). We ran the simulation for a total of 1000 milliseconds using forward Euler with a time step of $dt = 0.001$. Both activity and axial motion of the ROI are shown in the first row of Fig. S4B. At each time step t each beam recorded intensity from the sample according to the following equation:

$$I_j(t) = A(t)G_j(\Delta z(t)) \qquad \text{for } j = 1, 2, 3, 4 \tag{49}$$

where the functions $G_j(\Delta z(t))$ represent the integration of the excitation of each beam j at the ROI density. The intensities recorded by each beam are shown in the second row of Fig. S4.

To estimate the axial motion of the ROI, we extended the cost function for two beams (Eq. 19) and defined the following cost function for four beams:

$$J_{L_2}^{(4)}(z,t) =$$
$$\int_{-\infty}^{\infty} f(t'-t,\sigma_t)\left[\alpha_{12}\left(\frac{I_1(t)}{I_2(t)} - \frac{I_1^{stack}(z)}{I_2^{stack}(z)}\right)^2 + \alpha_{23}\left(\frac{I_2(t)}{I_3(t)} - \frac{I_2^{stack}(z)}{I_3^{stack}(z)}\right)^2 + \alpha_{34}\left(\frac{I_3(t)}{I_4(t)} - \frac{I_3^{stack}(z)}{I_4^{stack}(z)}\right)^2\right]dt', \tag{50}$$

where $f(t'-t,\sigma_t)$ is the Gaussian kernel defined by Eq. (20), and the parameters α_{12}, α_{23} and α_{34} are computed at each time step t defined as:

$$\alpha_{jk} = \begin{cases} 1 & \text{if} \quad I_j(t), I_k(t) > I_{th} \\ 0 & \text{otherwise,} \end{cases} \tag{51}$$

where $I_{th} = 0.1$ is a minimum intensity threshold. The parameters α_{jk} are used to only take into account measured intensities at t if the ROI is within the field of view of beams j and k. When the intensity recorded by one of the beams is lower than I_{th}, the ROI is considered outside of the z-field of view of the beam and therefore its contribution to the cost function of Eq. () is discarded by the α_{jk} parameters.

We estimated the axial motion of the single ROI by finding the slice in the stacks, $\Delta z(t)$, at any time step t, that minimized the cost function (). Both the estimated and actual axial motion are shown in Fig. S4B, third row. The cost function error, shown Fig. S4B, fourth row, is given by the value of the cost function evaluated at the estimated axial motion, $J^{(4)}_{L_2}(\Delta z(t), t)$.

Finally, the intensity of each beam is corrected using the following expression:

$$I_j^{cor}(t) = \frac{I_j(t)}{I_j^{stack}(\hat{z}(t))} \qquad \text{for } j = 1,2,3,4 \tag{52}$$

and the corrected fluorescence change, $\Delta F/F$ is computed from the corrected intensities:

$$\Delta F/F(t) = \frac{1}{4}\sum_{j=1}^{4}\left(\frac{I_j^{cor}(t) - F_j^0}{F_j^0}\right) \qquad \text{for } j = 1,2,3,4, \tag{53}$$

where F_j^0 is the baselines of the intensity I_j^{cor}, computed from the average of the 10% lowest values of $I_j^{cor}(t)$ for beam $j = 1,...,4$. The last row of Fig. S4B shows the corrected, actual, and measured $\Delta F/F$. The actual $\Delta F/F$ is computed according to Eq. 29. The measured $\Delta F/F$ is the fluorescence change that would be measured assuming no motion correction, given by:

$$\text{measured} \quad \Delta F/F = \frac{1}{4}\sum_{j=1}^{4}\frac{I_j(t) - I_j^0}{I_j^0}, \tag{54}$$

where I_j^0 is the baseline measured intensity, obtained by the mean value of the 10% lowest values of $I_j(t)$ for each beam $j = 1,...,4$.

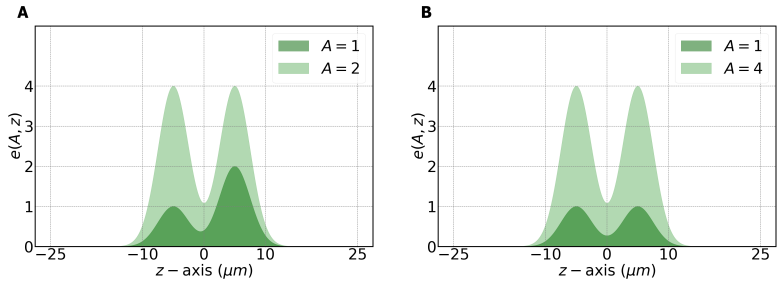

Fig. S1. Example of two different ROI functions. A ROI function defined by Eq. 8, where the activity A modulates heterogeneously the function along the z-axis. Such modulation can not be corrected with the developed algorithm. **B** ROI function defined by Eq. 12, where the activity A homogeneously modifies the ROI function along the z-axis. An underlying assumption of the algorithm is that activity is modulated in such a homogeneous fashion from baseline.

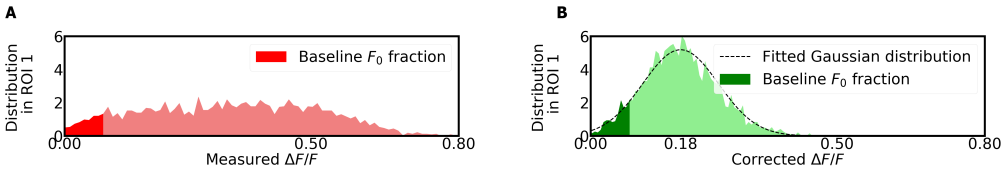

Fig. S2. Distributions of fluorescence changes for ROI 1 in the experiment shown in Fig. 4. **A** Distribution of the measured $\Delta F/F$ for ROI 1. This distribution is affected by axial motion. The distribution of the measured $\Delta F/F$ for ROI 1 is not Gaussian due to the axial motion **B** Gaussian distribution of the corrected $\Delta F/F$ for ROI 1. Since the fluorescence baseline is calculated from the average of 10% lowest values, the mean of the distribution of corrected $\Delta F/F$ is not centered around 0, as one would expect for GFP (no fluorescence changes).

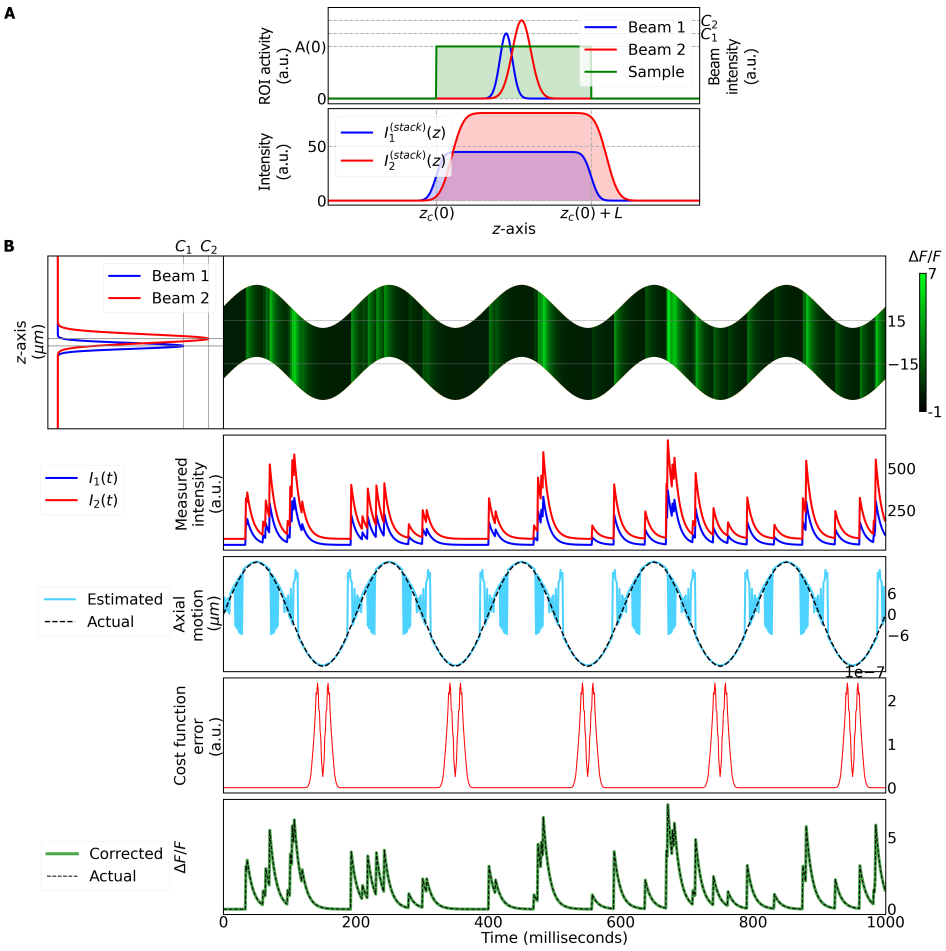

Fig. S3. Simulation of a single moving voxel stacks which have a flat axial profile. **A** Top row, defined flat and elongated ROI densities at time $t = 0$ as well as the profiles of the beams along the z-axis. Bottom row, stack of the sample at time $t = 0$ obtained for each beam. **B** First row, left side: profile of the two beams along the z-axis. Right side: activity and axial motion of the ROI over time. Second row: intensity measured with each beam over time. Third row: estimated and actual axial motion of the ROI over time. Fourth row: cost function error evaluated at the estimated axial position. Bottom row: measured, corrected and actual activity of the ROI over time.

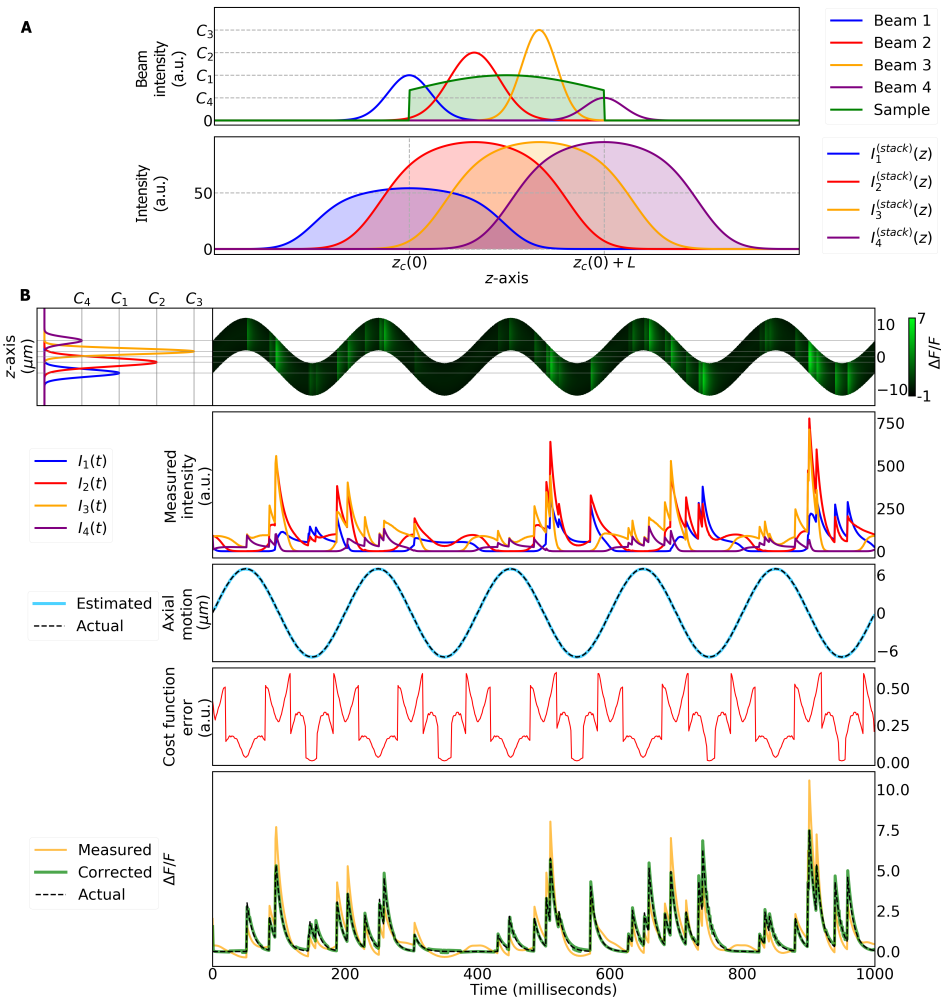

Fig. S4. Simulation of a single moving voxel for a configuration with four temporally mulitplexed beams. **A** Top row, ROI density at time $t = 0$ as well as the profiles of the four beams along the z-axis. Bottom row, stack of the sample at time $t = 0$ obtained for each beam. **B** First row, left side: profile of the four beams along the z-axis. Right side: activity and axial motion of the ROI over time. Second row: intensity measured with each beam over time. Third row: estimated and actual axial motion of the ROI over time. Fourth row: cost function error evaluated at the estimated axial position. Bottom row: measured, corrected and actual activity of the ROI over time.